Role of Electrical Charges on the Adsorption of Hydrogen: Something Old, Something New

G C Q da Silva, J M Simon, J. Marcos Salazar

Role of Electrical Charges on the Adsorption of Hydrogen: Something Old, Something New.

J. Marcos Salazar,* G. C. Q. da Silva, and J. M. Simon

Laboratoire ICB UMR 6303, Université Bourgogne Franche-Comté, 21078 Dijon, France

E-mail: *jmarcos@u-bourgogne.fr

Abstract

The adsorption of H_2 in zeolites by molecular simulations use, in many applications, single sphere model. Although this representation provides coherent results with experiments above 77K, below this temperature the usual hydrogen representation fails to reproduce experimental results. The disagreement can be associated to the interplay of the atomistic heterogeneity and the electric field produced by the zeolite faujasite. These aspects are generally excluded in classical force fields. For elucidating the influence of these issues, we performed DFT simulations for the faujasite $Na_{86}X$ at 40K with and without guest hydrogen molecules for determining the electrical field generated by the zeolitic structure. Our results show that the electrical field of the host structure induces a dipole moment on the hydrogens of ≈0.32 D. This value was included in classical Monte-Carlo simulations by using a dumbbell representation of H_2. Despite the small dipole moment, the simulations revealed an enhancement of adsorbed molecules. The formation of a dipolar moment in the H_2 suggests that at cryogenic temperatures the agreement with experiments passes through the use of polarizable models of H_2.

TOC Graphic

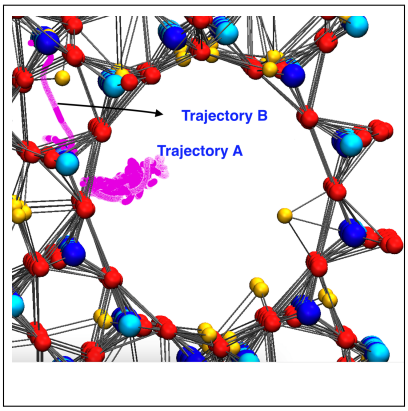

Introduction

The molecular hydrogen isotopes produced by nuclear processes require a recycling treatment for avoiding pollution or follow a molecular sieving treatment for a subsequent industrial use of H_2 and its isotopes. Heavy isotopes are mixed with hydrogen and is challenging to separate the molecular species. At cryogenic temperatures different solutions are available for separating hydrogen isotopes from gas mixtures. For instance, distillation[1] or adsorption in microporous material.[2–14] At these temperatures the physical chemical properties of hydrogen and its isotopes are well differentiated and is reflected by the de Broglie wavelength, that increases when temperature decreases. This effect, of quantum nature, depends on the atomic mass and is more pronounced for light species. Specifically, for hydrogen is reflected on a larger effective radius than for its isotopes.[2–4,15,16] In microporous materials this effect is large enough to generate distinct adsorption isotherms of H_2 and its isotopes. Furthermore, when dealing with mixtures at low temperatures (i.e., < 77K) it generates a selective adsorption of heavier isotopes. For zeolites this result has been highlighted by experiments[9,16] and molecular simulation.[17–24] Given that isotope selectivity is related to the differences in steric hindrance within the micropores, different zeolite types (e.g. shape, size, chemical formulation, etc.) have been compared for selecting the most ad-hoc materials for isotope separation.[9,10] These investigations revealed that cationic zeolites have a higher selectivity (up to 10 for Na-CHA at 47K) than its siliceous counterpart (3 for CHA under the same conditions).[24] For explaining the high selectivity several authors have assumed the presence of privileged adsorption sites (the cations).[9] This tendency lead to develop molecular simulations with potentials overestimating the cationic interaction[17] and without giving a satisfactory agreement with experiments below 70K.[17,22] As far as we know, the best agreement with experiments can be obtained by using a classical force field including the Feymann-Hibbs modification.[17–25] This approach includes a temperature dependence that mimics the de Broglie wavelength effect. Unfortunately, even with this correction the temperature dependence of the thermodynamic properties still without being reproduced

accurately below 77K. This rather awkward situation, lasting for more than two decades, lead us to reconsider the molecular hydrogen representation usually employed in molecular simulations and revisiting the outcomes from old experimental results.

A common practice, when modeling molecular H_2 by classical molecular simulations is to use a simple sphere model, a strategy reproducing reasonably well the observed thermodynamic adsorption properties above 77K. Below this temperature simulations and experiments mismatch. The force fields traditionally used neglect the molecular polarization and obviously the neutral sphere representation of H_2 too. Nonetheless, long time ago Crawford and Dagg[26] reported that the infrared spectra of molecular hydrogen in presence of a static electric field exhibits an absorption band originated by the dipole moment variation of H_2. Recently it has been shown that empirical potentials including an explicit polarization capture the best the energetics and they are useful for representing accurately the metal-framework interactions.[27]

In microporous materials like zeolites, the electric field generated by the structure can induce a molecular polarization of adsorbed molecules. Here we investigate these effects and we elucidate how the charge variability modifies the adsorption and diffusion processes in the $Na_{86}X$ of H_2. These studies are developed by using Ab Initio Molecular Dynamics (AIMD) and Monte-Carlo simulations at 47K.

Computational details

DFT Calculations

We analyzed the faujasite NaX with the Perdew-Burke-Ernzerhof (PBE)[28] generalized gradient approximation functional, associated with several additive dispersion correction schemes,[29] implemented in the VASP package[30] . The PAW scheme[29,31] was used to treat the electron-ion interactions. The plane wave cutoff energy was set to 500 eV. Given the large size of the unit cell, the Brillouin zone integration was performed with one Γ- point only. The

Kohn-Sham equations were solved self-consistently until the energy difference between cycles becomes lower than 10^{-8} eV. The atomic positions have been fully optimized until forces are smaller than 0.01 eV/Åper atom. For computing the interaction energies between H_2 molecules and the faujasite NaX accurately, we included the missing London dispersion interactions in conventional Kohn-Sham DFT with several vdW (van der Waals) correction schemes.[32,33]These methods include pairwise additive correction schemes of Grimme[34–36] . In this context, Tkatchenko and Scheffler (TS)[37] developed another approach based on the determination of C_6 according to the chemical environment. Here, we use the original TS scheme as well as the TS/HI version including an iterative Hirshfeld partitioning developed and implemented in VASP by Bučko and co-workers.[38–42]

Monte Carlo simulations

For calculating the adsorption isotherms of H_2 in the $Na_{86}X$ zeolite with the Monte Carlo technique, we used the DL_MONTE package[43,44] with the grand-canonical ensemble. The temperature imposed was 47 K and the fugacities range from 10 to 2.0×10^5 Pa.

The total simulation length consisted on more than 10^8 Monte Carlo steps encompassing: translation, rotation, insertion, and deletion moves. For extracting the average number of adsorbate molecules in the simulation box, the last 10 million cycles are used and representing 10^4 sampled configurations.

The simulation box consist of 8 unit cells (2 unit cells in each spatial direction) of the faujasite framework without adsorbate molecules. The zeolite was considered to be rigid and only displacements of cations(the sodium) and hydrogen molecules were allowed. Besides, the H-H bonds were also treated as rigid. The initial distribution of cation positions and Al substitutions were the same as used in our previous studies for the $Na_{86}X$.[22,23]

For accessing the effect of the atomic charges on the adsorption isotherms, different models for the hydrogen molecule are considered: I) a reference single-sphere model reported in previous works,[23] II) a dumbbell without any partial charges, III) a dumbbell presenting

a set of partial charges as reported by Pantatosaki *et al.*,[17] IV-VI) introduction in the H_2 of a charge imbalance of 0.01, 0.05 and 0.09, respectively.

The parameters of the chargeless dumbbell model (model I) were obtained by scaling all the pairwise Lennard-Jones interactions between the H_2 molecules and the zeolite atoms by a factor of two, since now there is the need for considering the interactions between atomic sites rather than between a whole molecule. This procedure could not be applied for the interaction between the H atoms themselves. Therefore, the Lennard-Jones parameters of Pantatosaki *et al.*[17] are used. The same set of Lennard-Jones interactions was also used in the models including partial charges. Throughout all the models, the interaction between the sodium cation and the oxygen of the zeolite were treated with a Buckingham potential and the parameters used are those given by Jaramillo *et al.*[45] In addition, the interaction among the cations themselves are described by a Lennard-Jones potential taken from ref.[22] and based on the parameters of Dang.[46]

For generating models with a permanent dipole on the hydrogen molecules, a charge imbalance was introduced by slightly modifying the original charge set of Pantatosaki *et al.*[17] The original model consist of two positive charges located at the atomic sites of the molecule and one negative charge at its center of mass, which accounts for interactions involving the quadrupole moment of H_2. Thus, the permanent dipoles are introduced by increasing one of the positive charges by 0.01, 0.05 and 0.09 and by decreasing the other one by exactly the same amount. The used parameters are tabulated in tables 2-5.

The Feynmann-Hibbs corrections[25] has been implemented to account for the quantum-mechanical contributions to the adsorption process.[22,23] A cut-off radius of 15 Å is employed for truncating both the Lennard-Jones, and the direct-space Coulomb potentials. The long-range electrostatic interactions are treated by means of the Ewald sum method with a precision of 10^{-6} in the energy. No long range corrections are applied to the dispersion interactions.

Table 1: Lennard-Jones parameters for the single sphere model as reported in ref.[23]

	ϵ (K)	σ (Å)
H_2 - H_2	38.00	2.920
H_2 - O	47.00	3.080
H_2 - Si	39.00	2.800
H_2 - Al	42.50	2.950
H_2 - Na	130.00	3.800
Na - Na	50.27	2.586

Table 2: Lennard-Jones parameters for all the dumbbell models considered in this work.

	ϵ (K)	σ (Å)
H - H[a]	14.50	2.500
H - O	23.50	3.080
H - Si	19.50	2.800
H - Al	21.25	2.950
H - Na	65.00	3.800
Na - Na	50.27	2.586

[a] Reported in ref.[17]

Table 3: Buckingham-potential parameters for the dispersion interaction between the cation and the zeolite Oxygen

A (K)	ρ (Å)	C (KÅ^6)
6.11558×10^7	0.2468	765898×10^5

Table 4: Partial charges of the atoms composing the adsorbent

q (e)			
O	Si	Al	Na
-1.3076	2.2341	2.0891	0.9960

Table 5: Sets of partial charges of the different dumbbell models of the adsorbate molecule

q (e)				
	Model III[a]	Model IV	Model V	Model VI
H1	0.4829	0.4929	0.5329	0.5729
H2	0.4829	0.4729	0.4329	0.3929
CM	-0.9658	-0.9658	-0.9658	-0.9658

[a] Extracted from ref.[17]

Results and discussion

Charge distribution: $Na_{86}X$

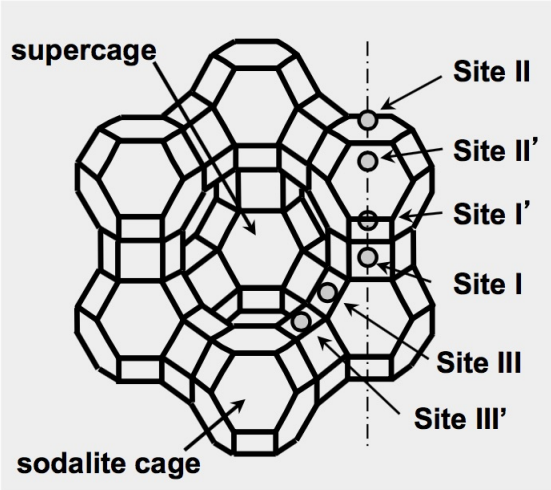

Figure 1: The three posible cation positions in the faujasite $Na_{86}X$. According to the cation disposition a non equal number of atoms in the eight surpercages is induced.

We performed DFT calculations for a unit cell of $Na_{86}X$ (662 atoms) faujasite for determining the net atomic charges (NAC). For this structure the whole unit cell counts eight supercages. In the $Na_{86}X$ each supercage has not the same number of atoms, this variability is due to the presence of cations in three different sites (Fig.1). The NAC calculations were performed by using the methodology proposed by T.A Manz in the package DDEC6.[47]

Having access to the NAC we can determine with ease the electrical field $E(r_j)$, generated by the $Na_{86}X$ at any position r_j inside the structure by using the following expression:

$$E(r_j) = \sum_{i=1}^{number\ of\ atoms} \frac{q_i \hat{r}_{ij}}{4\,\pi\epsilon_0 \mid \mathbf{r}_i - \mathbf{r}_j \mid^2} \qquad (1)$$

where q_i is the electric charge at $\mathbf{r}_i$. The calculated electric field of a H_2 placed at the center of a supercage of the $Na_{86}X$ is approximately of 1.2×10^{10} V/m. Interestingly, this value is of the same order of magnitude as the one reported by Cohen de Lara et al.,[48] for the NaA structure ($\approx 0.96 \times 10^{10}$ V/m). In Table.6 are given the calculated charge distribu-

tion of the faujasite analyzed and compared with those reported by Uytterhoeven *et al.,*[49] two decades ago. Our results show that the $Na_{86}X$ exhibits a large charge heterogeneity. Namely, the oxygens present a charge deviation of 27% from the mean value of ≈ -1.3077e (e= the elementary charge). This is a consequence of the Na and Al, surrounding the O, and responsible for the charge heterogeneity in the structure. This last implies steric movements affecting the adsorption of the adsorbent. Worthwhile to mention is that classical force fields give an excellent agreement with experimental isotherms above 77K.[17,22–24] Today, as far as we know, the best agreement with experiments is obtained with classical force fields including the Feymann-Hibbs quantum correction.[25] This modification gives a temperature dependence enhancing the agreement with experiments. However, for reproducing the thermodynamic properties below 77K this correction does not capture the physicochemical subtleties developing at cryogenic temperatures.

Electrical Charges

Table 6: Electrostatic charges calculated from DFT for the $Na_{86}X$.

Electrostatic charges (q)				
atoms	**Na**	**O**	**Al**	**Si**
NaX	$0.9967 \pm 1.95\%$	$-1.3077 \pm 27.4\%$	$2.0891 \pm 3.45\%$	$2.2341 \pm 4.5\%$
Uytterhoeven[49]	1.0	-0.8427	1.1498	1.3086

Single point energy calculations

As mentioned above Crawford and Dagg[26] reported an absorption band in the infrared spectra of molecular hydrogen in a static electric field. This suggests that adsorbed molecules can be polarized by the electric field generated by the zeolite. For corroborating this result we proceed by determine a potential energy surface of the $Na_{86}X$. For this we performed single point calculations by inserting H_2 molecules inside the eight SC (a total of 900 grid points homogeneously distributed). For each hydrogen molecule the potential energy and charge fluctuation are calculated. As expected, the lowest energies are for those points near

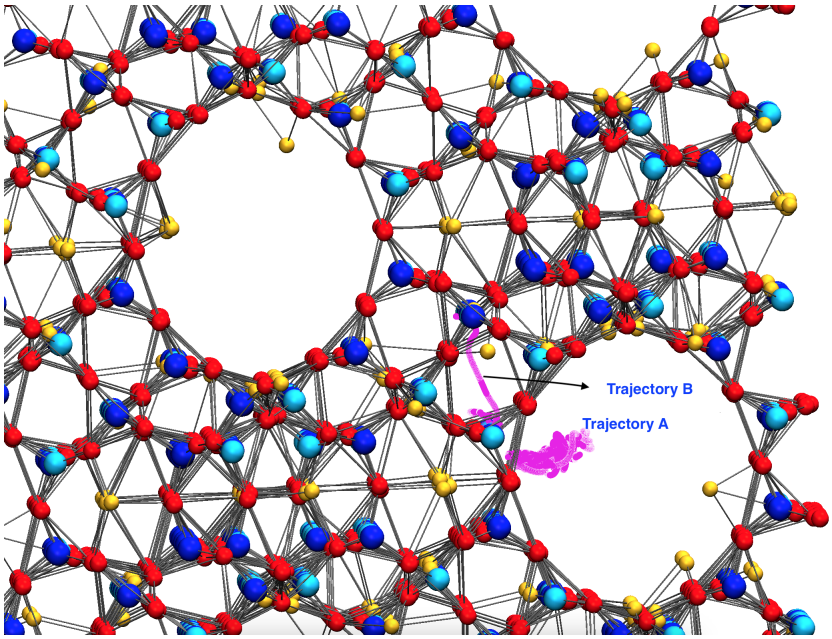

Figure 2: Two trajectories of 80 ps are depicted here. Trajectory A shows a H_2 near the supercage wall with steric displacements near its equilibrium position. Trajectory B shows displacements of fast particles. The figure shows that the color of the trajectory is not uniform, it has dark and light regions. Given that the trajectory is the superposition of frames in time, dark regions indicate that hydrogen molecules remains in a given position for a given lapse of time (between 6 and 10 ps). The NaX color representation is: Al (light blue), O(red), Na (green), Si(royal blue) and H_2 trajectories(magenta).

the SC walls (Table 7). Interestingly, the lower energy point is not always near the cation, it is the case for only three cases over eight.

The absolute values of the charge distribution of each H atom (of the H_2) located from the SC center to the walls varies from 0.083 to 0.093 e ($\approx$ 10% variation). With the H_2 molecules remaining neutral during the simulation. We quantified here the molecular dipole moment by the absolute value of the NAC on each hydrogen atom. The highest values are obtained for those molecules closer to the SC walls and with a dipole moment of ≈ 0.093 ($\approx 0.32D$).

These results clearly show that the electrical field of the zeolite polarized the hydrogen molecules and corroborate results given in ref.[26]

For elucidating how the electric field affects the amount of adsorbed H_2 we developed

Monte-Carlo simulations for the faujasite $Na_{86}X$ at 47K. We used a naive representation of the adsorbate by a dumbbell with a constant permanent dipole in the range [0.01,0.09] and we applied the Feynmann-Hibbs quantum correction. The interest of this representation of H_2 is to highlight the role of the polarization of H_2 on the adsorption isotherm. In Fig.3 the experimental values are represented by the solid continuous line, the single model (model I $\triangle$) shows that for pressures between 10 and 200 Pa (plain triangles) the model is in agreement with experimental values, however for higher pressures it tends to a saturation value. Consider a chargeless dumbbell for H_2 ($\triangledown$) given that the kinetic radius of the dumbbell is more cumbersome than a single sphere, the adsorbed amount of H_2 is reduced. Nonetheless, the form of the two curves are similar and tend to a saturation value of ≈ 16 H_2 per supercage ($\approx 25\%$ of its full capacity). Now, if we consider a quadrupole (model III in Table.4) the adsorption uptake is overestimated but crosses the experimental curve near 1000 Pa. As was mentioned in the previous paragraph the hydrogen molecules are polarized by the electrical charges of the atoms composing the faujasite structure. Now for the sake of comprehension of the role of charges let us impose, naively, to the hydrogen molecule a permanent dipole moment : 0.01 (model IV), 0.05 (model V) and 0.09 (model VI). The respective isotherms show that as the dipole moment is increased the experimental curve is crossed at higher pressures (green symbols) and the adsorption is enhanced and overestimated. If we focus on the experimental curve and the single sphere model at low pressures, between 10 and 200 Pa, it suggests that the van der Waals interactions between adsorbate molecules and the zeolite govern the adsorption process. As we increase in pressure our models III-VI exhibit an enhanced adsorption with the particularity of overestimating it. Nonetheless, they reveal an interesting feature: crossing the experimental curve at higher pressure as a function of the imposed dipole moment. When we impose a permanent dipole, and independently of the magnitude, the representation of the H_2 is far to be the most satisfactory. Nonetheless, it argues in favor of the use of polarizable models at cryogenic temperatures where the role of charges are leading the adsorption processes at pressures

above one thousand Pa.

Worthwhile to remark is that all the simulated isotherms tend to a saturation with the highest value around 18 H_2 per SC. This threshold number is far from the theoretical saturation value ($\approx$ 62 H_2). For explaining this discrepancy, let suppose a situation close to saturation. In this case the parameters governing the quantity of adsorbed molecules are: the pore volume and the interaction between the adsorbate molecules. The pore volume is commonly deduced from the saturation quantities and the pure adsorbate equation of state. Fig.4 gives the fugacity of H_2 computed from model III as a function of the density at 100K, 80K and 40K. They are compared with experimental results from.[50] Clearly for high temperatures ($>$ 77K) the simulated model is able to reproduce reasonably well the experimental equation of state (EOS). However at 40K the difference between experimental data and simulations is amplified. This highlights that the EOS at 40K is not properly described by the used model and as consequence the interactions between adsorbed molecules are not accurately modeled.

Thus, a perspective work would be the elaboration of a force field for the adsorbent that be compatible with polarizable models. Such models have the virtue of being more accurate for describing the H_2 EOS at cryogenic temperatures. Namely, the models proposed by Space and coworkers.[27]

Table 7: In this table we give the energy, dipole moment and the nearest neighbor of H_2 molecules placed at the supercage centers.

Energies and dipole moment of H_2		
Supercage/ atom	Energy (eV)	dipole moment
1 **O**	-0.47641E+4	-1.7354E-2/1.1483E-2
2 **Na**	-0.47561E+4	-9.17E-2/9.40E-2
3 **O**	-0.47561E+4	8.56E-2/-8.61-2
4 **O**	-0.47677E+4	8.34E-2/-8.35E-2
5 **Na**	-0.47561E+4	9.67E-2/-9.65E-2
6 **O**	-0.47561E+4	-8.38E-2/8.59E-2
7 **Na**	-0.47561E+4	-9.06E-2/8.68E-2
8 **O**	-0.47561E+4	-9.06E-2/9.24E-2

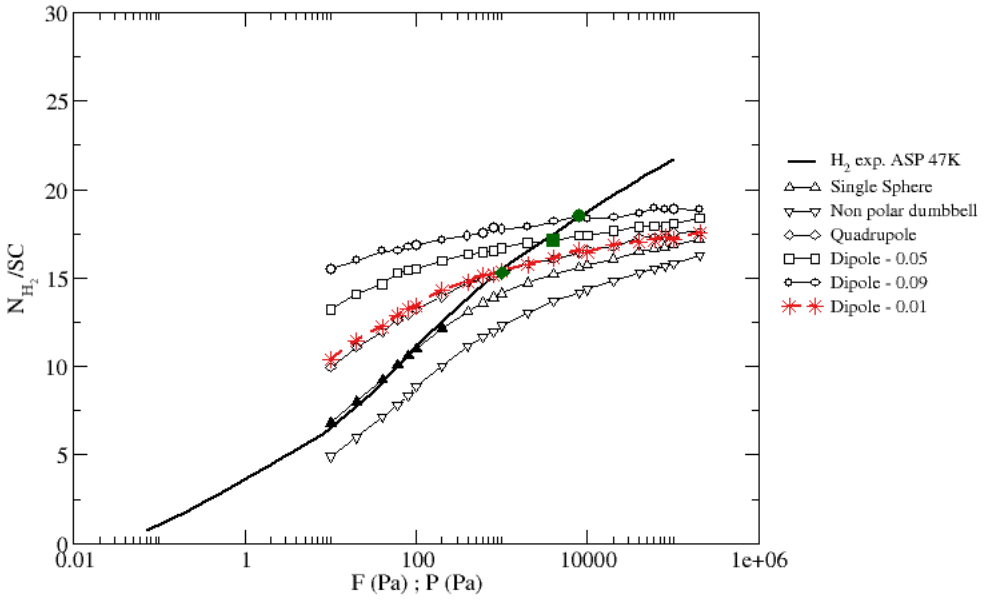

Figure 3: Adsorption isotherms of NaX at 47K by using different values of charges for the hydrogen.

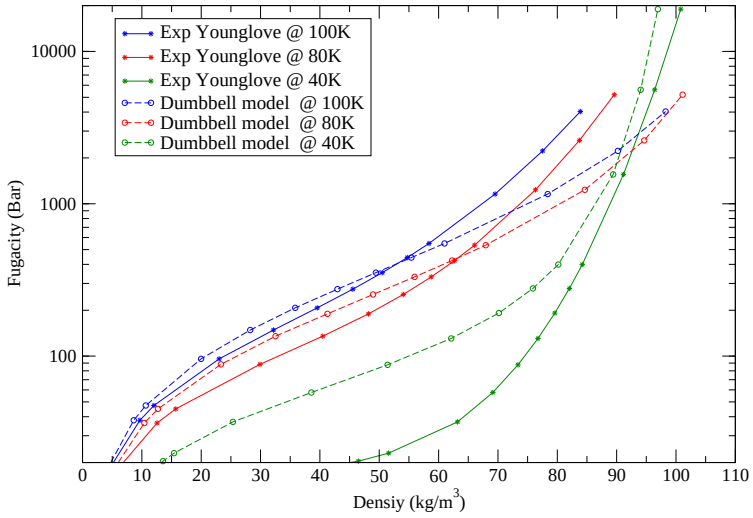

Figure 4: Experimental bulk fugacity of H_2 as a function of density compared to simulated data and results from a dumbbell model (Model III) and using a grand canonical Monte-Carlo program (see ref.[22])

Molecular diffusivity of H_2 in the NaX zeolite

We performed AIMD simulations at 40K for the $Na_{86}X$, including four or eight H_2 molecules per SC. The generated trajectories of 80 ps revealed that the majority of H_2 have their stable position near the SC walls, as expected. Interestingly, we identified two dynamical regimes:

A) Slow particles: Some particles can have erratic movements around a *sitting* position before jumping to another stable position. The calculated sitting times between jumps is approximately 2.7 ps. These particles contrast with those that once they reached a stable position near the SC wall do not move afterwards (trapped). Worthwhile to remark is that "trapped" particles are not always near the cation (Na^+). This is illustrated by the trajectory A in figure 2 where the H_2 moves around its sitting position.

B) Fast particles: These particles are characterized by long jumps from a residence (*sitting*) position to another. The fast particles have a sitting time of $\approx$ 0.3 ps and a jumping length between 1.6 and 2.0 Å (see the trajectory B in Fig. 2).
This behavior has been reported by quasi elastic neutron scattering[51] studies of H_2 in the NaA zeolite (from 70 to 150 K). Our studies suggest that the presence of slow and fast particles is a consequence of the atomistic charge heterogeneity governing the adsorbate-adsorbent interaction leading to this curious dynamical behavior.

Concluding remarks

We performed electronic structure calculations for studying the adsorption of H_2 on the faujasite $Na_{86}X$. Our analysis showed that hydrogen molecules are adsorbed preferentially close to the supercage walls, but not necessarily near the cations. The atomistic and energetic heterogeneities of such structure is enhanced by the presence of Al and Na^+ cations in three different possible sites. The electrical field produced by the zeolitic structure polarized the H_2 molecules and they acquire a dipole moment of $\approx$0.32 D. By performing Monte-Carlo simulations with a dumbbell representing for the hydrogen and by using the calculated dipole

moment, we obtained isotherms that are strongly dependent on the dipole strength.

Worthwhile to mention is, that our AIMD simulations reveled two distinct dynamical populations of molecules: slow and fast. With the former fluctuating $\approx$ 2.7 ps around a stable position near the faujasite walls for finally jumping to another supercage. The fast particles have a sitting time of $\approx$ 0.3 ps with a jumping length in the range of 1.6-2.0 Å. The interplay of the electrical field of the adsorbent and the dimensions of the porous structure produce populations of fast and slow particles governing the diffusion processes.

We also have shown, that the induced dipole moment of H_2 produced by the electrical field of the host structure can be determinant for having an agreement with experiments. In other words, the necessity of going beyond the non polarizable single sphere representation of the hydrogen.

Acknowledgments: We thank the CRI-CCUB Université de Bourgogne for giving us access to the computing facilities. We thank the EUR EIPHI and the region Bourgogne-Franche Comté for financial support.

References

(1) Rae, H. K., Ed. *Separation of Hydrogen Isotopes*; AMERICAN CHEMICAL SOCIETY, 1978.

(2) Beenakker, J.; Borman, V.; Krylov, S. Molecular transport in subnanometer pores: zero-point energy, reduced dimensionality and quantum sieving. *Chemical Physics Letters* **1995**, *232*, 379–382.

(3) Wang, Q.; Challa, S. R.; Sholl, D. S.; Johnson, J. K. Quantum Sieving in Carbon Nanotubes and Zeolites. *Phys. Rev. Lett.* **1999**, *82*, 956–959.

(4) Challa, S. R.; Sholl, D. S.; Johnson, J. K. Light isotope separation in carbon nanotubes through quantum molecular sieving. *Phys. Rev. B* **2001**, *63*, 245419.

(5) Challa, S. R.; Sholl, D. S.; Johnson, J. K. Adsorption and separation of hydrogen isotopes in carbon nanotubes: Multicomponent grand canonical Monte Carlo simulations. *The Journal of Chemical Physics* **2002**, *116*, 814–824.

(6) Kotoh, K.; Kudo, K. Multi-Component Adsorption Behavior of Hydrogen Isotopes on Zeolite 5A and 13X at 77.4 K. *Fusion Science and Technology* **2005**, *48*, 148–151.

(7) Kotoh, K.; Takashima, S.; Sakamoto, T.; Tsuge, T. Multi-component behaviors of hydrogen isotopes adsorbed on synthetic zeolites 4A and 5A at 77.4K and 87.3K. *Fusion Engineering and Design* **2010**, *85*, 1928–1934, Proceedings of the Ninth International Symposium on Fusion Nuclear Technology.

(8) Xiong, R.; Balderas Xicohténcatl, R.; Zhang, L.; Li, P.; Yao, Y.; Sang, G.; Chen, C.; Tang, T.; Luo, D.; Hirscher, M. Thermodynamics, kinetics and selectivity of H_2 and D_2 on zeolite 5A below 77K. *Microporous and Mesoporous Materials* **2018**, *264*, 22–27.

(9) Giraudet, M.; Bezverkhyy, I.; Weber, G.; Dirand, C.; Macaud, M.; Bellat, J.-P. D2/H2 adsorption selectivity on FAU zeolites at 77.4K: Influence of Si/Al ratio and cationic composition. *Microporous and Mesoporous Materials* **2018**, *270*, 211–219.

(10) Bezverkhyy, I.; Giraudet, M.; Dirand, C.; Macaud, M.; Bellat, J.-P. Enhancement of D_2/H_2 Selectivity in Zeolite A through Partial Na-K Exchange: Single-Gas and Coadsorption Studies at 45-77 K. *The Journal of Physical Chemistry C* **2020**, *124*, 24756–24764.

(11) Oh, H.; Savchenko, I.; Mavrandonakis, A.; Heine, T.; Hirscher, M. Highly Effective Hydrogen Isotope Separation in Nanoporous Metal-Organic Frameworks with Open Metal Sites: Direct Measurement and Theoretical Analysis. *ACS Nano* **2014**, *8*, 761–770.

(12) Weinrauch, I.; Savchenko, I.; Denysenko, D.; Souliou, S. M.; Kim, H.-H.; Tacon, M. L.; Daemen, L. L.; Cheng, Y.; Mavrandonakis, A.; Ramirez-Cuesta, A. J. et al. Capture of heavy hydrogen isotopes in a metal-organic framework with active Cu(I) sites. *Nature Communications* **2017**, *8*.

(13) Kim, J. Y.; Balderas-Xicohténcatl, R.; Zhang, L.; Kang, S. G.; Hirscher, M.; Oh, H.; Moon, H. R. Exploiting Diffusion Barrier and Chemical Affinity of Metal-Organic Frameworks for Efficient Hydrogen Isotope Separation. *Journal of the American Chemical Society* **2017**, *139*, 15135–15141.

(14) Kim, J. Y.; Zhang, L.; Balderas-Xicohténcatl, R.; Park, J.; Hirscher, M.; Moon, H. R.; Oh, H. Selective Hydrogen Isotope Separation via Breathing Transition in MIL-53(Al). *Journal of the American Chemical Society* **2017**, *139*, 17743–17746.

(15) Cai, J.; Xing, Y.; Zhao, X. Quantum sieving: feasibility and challenges for the separation of hydrogen isotopes in nanoporous materials. *RSC Adv.* **2012**, *2*, 8579–8586.

(16) Oh, H.; Hirscher, M. Quantum Sieving for Separation of Hydrogen Isotopes Using MOFs. *European Journal of Inorganic Chemistry* **2016**, *2016*, 4278–4289.

(17) Pantatosaki, E.; Papadopoulos, G. K.; Jobic, H.; Theodorou, D. N. Combined Atomistic Simulation and Quasielastic Neutron Scattering Study of the Low-Temperature Dynamics of Hydrogen and Deuterium Confined in NaX Zeolite. *The Journal of Physical Chemistry B* **2008**, *112*, 11708–11715.

(18) Kumar, A. V. A.; Jobic, H.; Bhatia, S. K. Quantum Effects on Adsorption and Diffusion of Hydrogen and Deuterium in Microporous Materials. *The Journal of Physical Chemistry B* **2006**, *110*, 16666–16671.

(19) Kumar, A. V. A.; Jobic, H.; Bhatia, S. K. Quantum effect induced kinetic molecular sieving of hydrogen and deuterium in microporous materials. *Adsorption* **2007**, *13*, 501–508.

(20) Perez-Carbajo, J.; Parra, J. B.; Ania, C. O.; Merkling, P. J.; Calero, S. Molecular Sieves for the Separation of Hydrogen Isotopes. *ACS Applied Materials & Interfaces* **2019**, *11*, 18833–18840.

(21) Deeg, K. S.; Gutiérrez-Sevillano, J. J.; Bueno-Pérez, R.; Parra, J. B.; Ania, C. O.; Doblaré, M.; Calero, S. Insights on the Molecular Mechanisms of Hydrogen Adsorption in Zeolites. *The Journal of Physical Chemistry C* **2013**, *117*, 14374–14380.

(22) Salazar, J.; Lectez, S.; Gauvin, C.; Macaud, M.; Bellat, J.; Weber, G.; Bezverkhyy, I.; Simon, J. Adsorption of hydrogen isotopes in the zeolite NaX: Experiments and simulations. *International Journal of Hydrogen Energy* **2017**, *42*, 13099–13110.

(23) Salazar, J. M.; Badawi, M.; Radola, B.; Macaud, M.; Simon, J. M. Quantum Effects on the Diffusivity of Hydrogen Isotopes in Zeolites. *The Journal of Physical Chemistry C* **2019**, *123*, 23455–23463.

(24) Radola, B.; Bezverkhyy, I.; Simon, J.-M.; Salazar, J. M.; Macaud, M.; Bellat, J.-P. Enhanced quantum sieving of hydrogen isotopes via molecular rearrangement of the adsorbed phase in chabazite. *Chemical Communications* **2020**, *56*, 5564–5566.

(25) Feynman, R. *Quantum mechanics and path integrals*; Dover Publications: Mineola, N.Y, 2010.

(26) Crawford, M. F.; Dagg, I. R. Infrared Absorption Induced by Static Electric Fields. *Phys. Rev.* **1953**, *91*, 1569–1570.

(27) Hogan, A.; Space, B. Next-Generation Accurate, Transferable, and Polarizable Potentials for Material Simulations. *Journal of Chemical Theory and Computation* **2020**, *16*, 7632–7644.

(28) Perdew, J.; Burke, K.; Ernzerhof, M. Generalized Gradient Approximation Made Simple. *Phys Rev Lett* **1996**, *77*, 3865–3868.

(29) Kresse, G.; Hafner, J. Ab initio molecular dynamics for liquid metals. *Phys Rev B* **1993**, *47*, 558–561.

(30) Hafner, J. Ab-Initio Simulations of Materials Using VASP: Density-Functional Theory and Beyond. *J. Comput. Chem.* **2008**, *29*, 2044–2078.

(31) Blöchl, P. Projector Augmented-Wave Method. *Phys. Rev. B* **1994**, *50*, 17953–17979.

(32) Chebbi, M.; Chibani, S.; Paul, J.; Cantrel, L.; Badawi, M. Evaluation of volatile iodine trapping in presence of contaminants: A periodic DFT study on cation exchanged-faujasite. *Microporous Mesoporous Mater* **2017**, *239*, 111–122.

(33) Hessou, E.; Kanhounnon, W.; Rocca, D.; Monnier, H.; Vallières, C.; Lebègue, S.; Badawi, M. Adsorption of NO, NO2, CO, H2O and CO2 over Isolated Monovalent Cations in Faujasite Zeolite: A Periodic DFT Investigation. *Theor Chem Acc* **2018**, *137*, 161.

(34) Grimme, S. Semiempirical GGA-type density functional constructed with a long-range dispersion correction. *J Comput Chem* **2006**, *27*, 1787–1799.

(35) Grimme, S.; Antony, J.; Ehrlich, S.; Krieg, A Consistent and Accurate Ab Initio Parametrization of Density Functional Dispersion Correction (DFT-D) for the 94 Elements H-Pu. *Journal of Chemical Physics* **2010**, *132*, 154104.

(36) Grimme, S.; Ehrlich, S.; Goerigk, L. Effect of the Damping Function in Dispersion Corrected Density Functional Theory. *J. Comput. Chem* **2011**, *32*, 1456–1465.

(37) Tkatchenko A, S. M. Accurate Molecular Van Der Waals Interactions from Ground-State Electron Density and Free-Atom Reference Data. *Phys Rev Lett* **2009**, *102*, 073005.

(38) Bučko, T.; Lebègue, S.; Hafner, J.; Ángyan, J. G. Tkatchenko-Scheffler van Der Waals

Correction Method with and without Self-Consistent Screening Applied to Solids. *Phys. Rev. B* **2013**, *87*, 064110.

(39) Bučko, T.; Lebègue, S.; Hafner, J.; Ángyan, J. G. Improved Density Dependent Correction for the Description of London Dispersion Forces. *J Chem Theory Comput* **2013**, *9*, 4293–4299.

(40) Bučko, T.; Lebègue, S.; Ángyan, J. G.; Hafner, J. Extending the applicability of the Tkatchenko-Scheffler dispersion correction via iterative Hirshfeld partitioning. *Journal of Chemical Physics* **2014**, *141*, 034114.

(41) Gould, T.; Lebègue, S.; Ángyan, J. G.; Bučko, T. Fractionally Ionic Approach to Polarizability and van der Waals Many-Body Dispersion Calculations. *J Chem Theory Comput* **2016**, *12*, 5920–5930.

(42) Bučko, T.; Hafner, J.; Lebègue, S.; Ángyan, J. G. Improved Description of the Structure of Molecular and Layered Crystals: Ab Initio DFT Calculations with van Der Waals Corrections. *J. Phys. Chem. A* **2010**, *114*, 11814–11824.

(43) Brukhno, A. V.; Grant, J.; Underwood, T. L.; Stratford, K.; Parker, S. C.; Purton, J. A.; Wilding, N. B. DL_MONTE: a multipurpose code for Monte Carlo simulation. *Molecular Simulation* **2019**, *47*, 131–151.

(44) Purton, J.; Crabtree, J.; Parker, S. DL_MONTE: a general purpose program for parallel Monte Carlo simulation. *Molecular Simulation* **2013**, *39*, 1240–1252.

(45) Jaramillo, E.; Auerbach, S. M. New Force Field for Na Cations in Faujasite-Type Zeolites. *The Journal of Physical Chemistry B* **1999**, *103*, 9589–9594.

(46) Dang, L. X. Mechanism and Thermodynamics of Ion Selectivity in Aqueous Solutions of 18-Crown-6 Ether: A Molecular Dynamics Study. *Journal of the American Chemical Society* **1995**, *117*, 6954–6960.

(47) Manz, T. A.; Limas, N. G. Introducing DDEC6 atomic population analysis: part 1. Charge partitioning theory and methodology. *RSC Advances* **2016**, *6*, 47771–47801.

(48) Stéphanie-Victoire, F.; Cohen de Lara, E. Adsorption and coadsorption of molecular hydrogen isotopes in zeolites. II. Infrared analyses of H_2, HD, and D_2 in NaA. *The Journal of Chemical Physics* **1998**, *109*, 6469–6475.

(49) Uytterhoeven, L.; Dompas, D.; Mortier, W. J. Theoretical investigations on the interaction of benzene with faujasite. *J. Chem. Soc., Faraday Trans.* **1992**, *88*, 2753–2760.

(50) Younglove, B. A. *Thermophysical properties of fluids*; Journal of Physical and Chemical Referene Data Supplements; American Institute of Physics: New York, NY, 1982.

(51) De Lara, E. C.; Kahn, R. Diffusivity of the deuterated hydrogen molecule HD in NaA zeolite by neutron scattering experiment. Comparison with H2 in NaA. *The Journal of Chemical Physics* **1992**, *96*, 862–863.